Journal Name

ARTICLE

The Bioconjugation Mechanism of Purine Cross-linkers Affects Microstructure and Cell Response to Ultra Rapidly Gelling Purine-Chitosan Sponges

Received 00th January 20xx,
Accepted 00th January 20xx

DOI: 10.1039/x0xx00000x

www.rsc.org/

Laila Benameur[a,‡], Timothée Baudequin[a,‡], Mina Mekhail[a,c], Maryam Tabrizian[a,b,*]

ABSTRACT: To be used as cell carrier, cross-linking is one of the most common approaches to provide chitosan with more structural integrity. We introduced a cross-linking strategy through using two purines, guanosine 5'-diphosphate (GDP) or adenosine 5'-diphosphate (ADP), as cross-linkers. The rationale for this approach is that both GDP and ADP have an important physiological role, and act as intercellular signaling molecules in many biological processes. The slightly difference between the chemical structure of guanine and adenosine in GDP and ADP respectively affected the cross-linking mechanism. As a result, it led to a different scaffold microstructure, and thereby altered the response of encapsulated cells to the scaffold. FTIR and solid-state ^{13}C-NMR revealed the formation of a quadruplex structure among four GDP molecules confined between chitosan backbone. This was as a result of the guanine ability to form hydrogen bonds with each other, while adenosine in ADP lacks this capacity. The formation of more organized structure in GDP-chitosan sponges also increased the crystallinity of the sponge as shown by X-Ray Diffraction. Further physicochemical analyses with SEM and µCT indicated a more open pores' architecture and increased porosity. While an active population of encapsulated cells was maintained in all the chitosan sponges over time, the GDP-based sponges provided a 6-fold increase in MC-3T3 cells' activity and enhanced significantly their proliferation due to the more seemly microstructure. Overall findings suggest that slight changes in chemical structure of cross-linker for the preparation of chitosan-based biomaterials will have a significant impact on the structural properties of the chitosan. This could be used as an important parameter for modulating cell response and to understand the cell signaling pathway to chitosan-based biomaterials in the context of their applications in tissue engineering.

[a] *Department of Biomedical Engineering, McGill University, Montreal, Quebec, Canada.*
[b] *Faculty of Dentistry, McGill University, Montreal, Quebec, Canada.*
[c] *Current address: Shriners Hospitals for Children, Montreal, Quebec, Canada.*
‡ These authors contributed equally.
*Corresponding author: Maryam Tabrizian, McGill University, Department of Biomedical Engineering, 3775, Rue University, Room 313/308B, Montréal, QC H3A 2B4, Canada.
Email: maryam.tabrizian@mcgill.ca
Electronic Supplementary Information (ESI) available: [NMR prediction spectra, XRD spectra, µCT measurements and, DAPI staining on frozen sections of the chitosan sponges with encapsulated cells]. See DOI: 10.1039/x0xx00000x

This journal is © The Royal Society of Chemistry 20xx

Please do not adjust margins

INTRODUCTION

Over the past few decades, to better understand the role of scaffolds in tissue engineering approaches, this field of research has received a great deal of attention. The most recent investigations seek to use the scaffolds for stem cell therapy. To be used as such, there is an increasing need to develop methods and protocol for their use as delivery systems and for cell encapsulation [1–3]. In the context of bone tissue engineering, an important therapeutic strategy is the use of biocompatible scaffolds made of natural and synthetic polymers that can facilitate bone repair, biomineralization and bone tissue regeneration[4–6]. In addition to biocompatibility and the need for working in controlled culture, an ideal scaffold for bone regeneration must meet some other specific requirements such as biodegradability, low immunogenicity, appropriate mechanical properties and microstructure (high porosity with connectivity similar to natural bone)[7,8] to promote bone growth into interconnected pores.

Among natural polymers, the chitosan-based scaffolds have been shown to meet most of these requirements and are currently employed as hydrogel matrices for an array of medical and pharmaceutical applications**,** particularly as therapeutic drug and cell delivery vehicles[5,9–12]. The chitosan is an aminated polysaccharide consisting of N-acetyl-D-glucosamine and D-glucosamine units. It is considered to be a naturally occurring cationic biopolymer due to the protonation of the amino groups, thus making chitosan chemically highly reactive and allowing further chemical modifications[13,14]. Cross-linking is one of the most common strategies to provide chitosan with more structural integrity. This approach has been validated with various cross-linkers such as genipin, formaldehyde or sodium tripolyphosphate[15–17]. The choice of cross-linker was found to modify the kinetic release of encapsulated drugs and allowed the fabrication of scaffolds promoting cell adhesion[15,16]. In a previous work, we developed an injectable, rapidly-gelling chitosan sponge using purine, namely guanosine 5'-diphosphate (GDP) for the first time as ionic cross-linker, with promising properties as a drug delivery system and as a scaffold to promote biomineralization[18,19].

Using this cross-linker, the formation of the chitosan sponge occurs in less than 2 seconds, and this is the most rapidly-gelling chitosan system so far reported in the literature either with another cross-linker or by any other physical or chemical means. Unlike most current injectable hydrogels, no external trigger such as temperature, pH, UV-irradiation or chemical cross-linking agents are required to initiate the gelation process and the homogeneous formation of the sponge[20–25]. The advantage of such a fast-gelling system is the implantation of the scaffold at the site of injury using *in-situ* injection, thus avoiding undesired leakage and ensuring a minimally invasive surgical procedure. We successfully used the GDP-based chitosan sponge to deliver biologically active molecules such as growth factors with high encapsulation efficiency and slow release to prolong the effect of functional regulators[19,26]. We also showed the beneficial effects of this scaffold on biomineralization of pre-osteoblasts cells[19] and on oligodendrocyte progenitor cells' attachment and differentiation[18]. These findings indicated that these chitosan sponges are suitable matrices for a wide range of tissue engineering applications. To further support this statement, in this work, we aimed at using chitosan sponge as scaffold for cell encapsulation and to determine the structural parameters that affect cell response in this confined microenvironment.

There is a general agreement that a three-dimensional environment with an adequate microstructure is crucial for bone cell encapsulation in order to protect cells from mechanical stress and to promote cell adhesion, proliferation, pre-vascularization and driving tissue regeneration, as well as to support an adequate oxygen exchange and nutrient flow diffusion[27,28]. However, understanding the microstructural and microarchitectural effects and separating them from other structural parameters remains an unmet goal for bone tissue engineering.

In order to emphasize the fate of chitosan sponge microstructure and isolate this effect from other structural parameters, we constructed the chitosan sponges using two purine materials, GDP as well as adenosine 5'-diphosphate (ADP), another ionic cross-linking agent. Similar to GDP-based chitosan sponges, the gelation occurs through phosphate-amine interactions of purine and chitosan respectively, in 2 to 3 seconds.

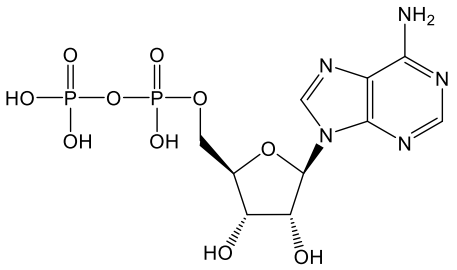

Adenosine 5'-diphosphate (ADP)

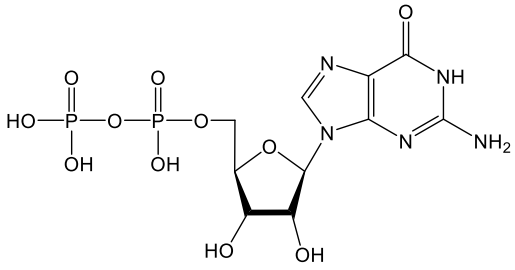

Guanosine 5'-diphosphate (GDP)

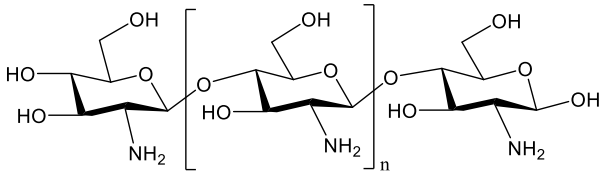

Chitosan

Figure 1. Chemical structures of Adenosine 5'-diphosphate (ADP), guanosine 5'-Diphosphate (GDP) and chitosan.

This journal is © The Royal Society of Chemistry 20xx

Please do not adjust margins

Using ADP as a new alternative cross-linker allowing the same rapid gelation rate, was therefore sought as a mean to modify the microstructure of the sponge, in order to analyse its influence on encapsulated cell behaviour compared to GDP-based sponges. The hypothesis was that the slightly different chemical structures between the two purines will result in significant difference in the sponge microarchitecture (Figure 1), and that this difference will alter the behaviour of pre-osteoblast MC-3T3 cells encapsulated in the scaffolds. Changes would therefore be as a result of variations in microenvironment provided by GDP- and ADP-based sponges. This strategy also provided us with the opportunity to focus on two research questions: 1) how cells will sense the small difference in the chemical composition of the cross-linkers and respond accordingly to these two sponge formulations, and 2) knowing that both GDP and ADP have important physiological roles and act as intercellular signalling molecules in a wide range of biological processes, particularly in the regulation of bone metabolism and development as well as in tissue protection[29–31] but through two different signalling pathway of osteogenesis[29,32,33], how the encapsulated pre-osteoblast response will be affected in these purine-based sponges.

Four sponge formulations, varying in the type of cross-linker, or pH and concentration of chitosan solutions were constructed. Their physicochemical properties were fully characterized by Fourier transform infrared spectroscopy, X-ray diffraction and solid-state ^{13}C-NMR to resolve the bioconjugation mechanism between the chitosan and purines that would imply structural differences between GDP- and ADP-based sponges. To delineate the effect of cross-linking mechanisms in instigating changes in bulk morphology, micro-computed tomography analysis was performed to determine porosity and surface/volume ratio of the different sponge formulations. The metabolic activity and proliferation of pre-osteoblast cells MC-3T3 encapsulated in the chitosan sponges prepared either with ADP or GDP were investigated. In complement to these analyses, the microstructural features of the sponges as well as cell attachment were observed by scanning electron microscopy and confocal microscopy with and without encapsulated cells. The biological behaviour of the cell-encapsulated sponge was assessed with Alamar Blue assay after 1, 4 and 7 days of culture. We investigated how the biological response of the encapsulated pre-osteoblasts was influenced by the cross-linker solution used to form the scaffold, and performed a cross-analysis with the internal and molecular structures of the chitosan sponges to consolidate our hypothesis on the cross-linking mechanisms.

EXPERIMENTAL

Materials

High Molecular Weight Chitosan (Degree of Deacetylation >90%; 3000 cp viscosity, average molecular weight 100,000 - 300,000 g/mol) was purchased from MP Biomedicals, LLC; guanosine 5'-diphosphate (GDP) sodium salt, adenosine 5'-diphosphate (ADP) sodium salt, and bovine serum albumin (BSA) from Sigma Aldrich; Hydrochloric Acid (50% v/v) from LabChem Inc; MC-3T3-E1 cell line from ATCC; Minimum Essential Medium (MEM-Alpha), Fetal Bovine Serum (FBS), Penicillin-Streptomycin, Alamar Blue and Quant-iT Picogreen dsDNA assay kit from Invitrogen; Dulbecco's phosphate buffered saline without calcium or magnesium (DPBS$^-$), Paraformaldehyde, Sodium Bicarbonate, Superfrost Plus Microscope Slides, Sucrose, Alexa Fluor® 647 Phalloidin, diamidino-2-phenylindole (DAPI) and mounting medium with DAPI from Thermo Fisher Scientific, Clear Frozen Section Compound from VWR.

Chitosan sponge construction

For the preparation of the chitosan sponges, a slightly modified version of the protocol previously reported by the authors was used[18]. Briefly, 3- and 6-mg/ml chitosan solutions were prepared by dissolving the chitosan in 0.06 M HCl under magnetic stirring for 30 min. The pH of the solution was adjusted to 5 or 6 using a 1 M sodium bicarbonate solution. Cross-linker solutions (100 mg/ml) were prepared by dissolving either GDP or ADP salts in cell culture medium without FBS. Prior to sponge fabrication, chitosan, GDP and ADP solutions were sterilized by filtration through 0.22-µm syringe filters. Sponges were formed by pouring cross-linker to chitosan solution in a 2-mL microtube. The formation of sponge occurs immediately and gentle physical mixing of the tube content ensures the formation of a single piece of round-shaped scaffold. Four formulations of sponge varying in chitosan concentration and pH of chitosan solution as well as the type of cross-linker were obtained (Table 1).

Table 1. Chitosan sponges used in this study.

Sponge Abbreviation	Cross-linker	[Chitosan] mg/mL	pH
GDP C3PH5	GDP	3	5
ADP C3PH5	ADP	3	5
GDP C6PH6	GDP	6	6
ADP C6PH6	ADP	6	6

Fourier Transform Infrared (FTIR) spectroscopy

FTIR spectroscopy (Perkin Elmer, Pike Technologies) was performed on different formulations of the chitosan sponges as well as on pure chitosan, GDP, and ADP powders. The spectra were collected in absorption mode between 4000 and 400 cm^{-1}, using 64 scans, and a resolution of 4 cm^{-1}.

X-Ray Diffraction (XRD)

Chitosan sponges were lyophilized using a Thermo Savant ModulyoD freeze dryer to obtain sample powders. XRD analysis was performed on different formulations of the chitosan sponges as well as on pure chitosan, GDP, and ADP powders. A D8 Discover device (Bruker) was used with a Copper X-ray source to evaluate the degree of crystallinity of the samples.

Magic angle ^{13}C-Nuclear Magnetic Resonance (NMR) spectroscopy

The sample powders as obtained for XRD were used for NMR analyses. All spectra were acquired with a Varian VNMRS 400 MHz NMR spectrometer for ^{13}C using a wide bore 4mm T3 double-resonance probe spinning at 13 kHz. The pulse

Please do not adjust margins

sequence consisted in a multiCP sequence[34] with 10 periods of CP of 1 ms, each separated by 500 ms delay. The recycle delay was 3 s. 1024 scans were acquired. Spectra were referenced to the carbonyl ^{13}C signal of glycine at 176.04 ppm.

Micro-Computed Tomography (μCT)

The three-dimensional (3-D) architecture and microstructural features of chitosan sponges with or without encapsulated cells were assessed by μCT after 1, 4 or 7 days. The samples were rinsed with sterile PBS, fixed for 30 minutes in 4% paraformaldehyde and dehydrated by successive immersions in ethanol and amyl-acetate baths. Critical point drying was performed using Leica EM CPD030 to dehydrate the samples. Measurements were performed using Skyscan 1272 High-resolution micro-CT (Bruker, Germany) with 35 kV, 231 μA, a pixel size of 2.5 μm and a 4K resolution. 3-D models of the sponges were reconstructed from the 2-D acquisitions with the NRecon software and analysed with the CTAn software (Bruker, Germany). For each individual sponge, three samples (0.25-mm thickness, 1.75-mm diameter) were then randomly chosen and analysed to determine their porosity, pore connectivity, and surface/volume ratio. According to the documentation available for the software (http://bruker-microct.com/next/CTAn03.pdf as consulted on November 6th, 2017), pore connectivity is the degree to which parts of the object are multiply connected. It is a measure of the number of connections in a pore network required to maintain parts of an object together before the structure falls into two separate pieces. In a 3D model, a closed pore is defined as a connected assemblage of space empty units that is fully surrounded on all sides in 3-D by solid units.

MC-3T3 pre-osteoblasts culture and encapsulation

Mouse pre-osteoblasts MC-3T3 were first expanded in complete proliferation medium containing alpha-MEM supplemented with 10% FBS and 1% Penicillin-streptomycin. Pre-osteoblasts with 80–85% confluence were then trypsinised and counted for the encapsulation step. For all formulations, 0.1 ml of cell suspension containing 5 x 10^5 MC-3T3 was added to 0.3 ml of either ADP or GDP solutions prior to the gelation step. The cell-cross-linker suspension was rapidly poured into the vial containing 1.6 ml of chitosan solution to form the sponge. The formed chitosan sponge encapsulating cells was immediately removed from the remaining solution using tweezers, placed in 48-well plates and rinsed three times with complete alpha-MEM medium for 15 min to bring the cellular environment to physiological pH.

Scanning electron microscopy analysis (SEM)

Chitosan sponges containing cells were kept in proliferation medium for 1, 4 or 7 days and processed as described for the μCT analyses to obtain dehydrated samples. After critical point drying, the sponges were cut in half and coated with Gold/Palladium. The structural morphology of the sponges, as well as the spreading pattern and the morphology of the cells, were observed with a Hitachi S-4700 Field Emission Scanning Electron Microscope at 2 keV and 10 μA.

Assessment of encapsulated MC-3T3 cells' metabolic activity and proliferation

The Alamar Blue assay was performed to assess the metabolic activity and proliferation of MC-3T3 cells encapsulated into different formulations of chitosan sponges. ADP C3PH5, ADP C6PH6, GDP C3PH5 and GDP C6PH6 containing 5 × 10^5 MC-3T3 cells were placed in triplicate on 48-well plates with complete proliferation medium. Chitosan sponges without cells were used as blank and controls. After 1, 4, and 7 days of culture, cells were incubated in 10% Alamar Blue/alpha-MEM (without phenol red) solution in a humidified atmosphere at 37°C and 5% CO_2. Following a 4-hour incubation, 100 μl of supernatant were transferred to 96-well plates and measured at 560 nm (excitation) and 590 nm (emission) to determine the percentage of Alamar Blue reduction using spectrophotometry (SpectraMax i3, SoftMax Pro 6.3).

Sponge degradation and DNA quantification

The chitosan sponges were degraded by incubating the samples in PBS containing 200 mg/ml of lysozyme, at 37°C under stirring in incubator. 500 μl of lysis buffer were added to the tubes and the cell lysates were examined for double stranded DNA to quantify the cell number. The assay was performed as per the manufacturer's instructions (Quant-iT PicoGreen assay kit). In brief, 50-μL aliquots of the cell lysates were added in a 96-well assay plate. 50 μL of a 1:200 dilution of picogreen were added to each well and incubated for 5 min in the dark. The assay plate was read at 480 nm excitation and 520 nm emission using spectrophotometry (SpectraMax i3, SoftMax Pro 6.3). The DNA concentration was determined using the standard curve obtained with a dsDNA standard sample. Results were used to normalize the metabolic activity measurements of the encapsulated cells.

Phalloidin and DAPI immunofluorescence staining

The cells encapsulated into the different sponges were kept in complete proliferation medium for 1, 4, and 7 days. The sponges were washed thoroughly with DPBS after each time point and fixed in 4% paraformaldehyde for 15 min.

For phalloidin staining, the fixed samples, permeabilized with 0.2% Triton X-100 detergent for 3 min, were incubated for 1h with Alexa Fluor® 647-conjugated phalloidin (1/1000) for F-actin labelling and with DAPI (1/5000) for nuclear staining. The images were collected using LSM710 Laser Scanning Confocal Microscope (Carl Zeiss Canada) and image analysis was performed using Imaris 8.3 Software (Bitplane, Oxford Instrument).

For DAPI staining of frozen sections, the fixed samples were immersed in a Section Compound:30%wt/v sucrose (2:1) solution and then placed in liquid nitrogen until the formation of solid blocks. Frozen sections were cut with a Bright OTF Cryostat microtome (Bright Instruments, 10-μm thickness, 5° angle) and fixed on slides. Cover glasses were prepared with a DAPI-containing mounting medium and the slides were observed with a Leica DMRB fluorescence microscope (Leica Microsystems) to determine the cell distribution homogeneity.

Statistical analysis

All experiments were done in triplicates (n=3 independent experiments). One-way ANOVA with Tukey's test was used to

This journal is © The Royal Society of Chemistry 20xx

Please do not adjust margins

assess the significant differences between the groups with 95% confidence.

RESULTS AND DISCUSSION

The chemistry of purine determines the cross-linking mechanism of chitosan

FTIR and solid ^{13}C-NMR allowed to determine the bioconjugation mechanism of GDP and ADP to chitosan backbone. **Error! Reference source not found.**A and B show the FTIR spectra of chitosan, ADP, and GDP. The positions of representative peaks in the chitosan spectrum were in agreement with previous reports[17,35]. The chitosan characteristic peak that appeared at 1645 cm^{-1} was attributed to the amide I C=O stretching vibration and the peak at 1588 cm^{-1} to the amide II bending vibration of N-H. The broad absorption band in the region of 3400-3500 cm and 3440 cm^{-1} were assigned respectively to the O-H group stretching vibration and to the stretching vibration of N-H[36] in chitosan powder. As expected, ADP and GDP yielded the same major peaks. Both molecules showed characteristic absorption peaks at 903 cm^{-1} due to the pyrophosphate (P-O-P) groups in purine, at 1100 cm^{-1} for the P-O stretching vibration and at 1222 cm^{-1} for the P=O group[37–39]. The peaks of ADP and GDP above 1300 cm^{-1} were mainly assigned to the adenine, guanine and ribose part of the nucleotides[40]. For the ADP, the C-(NH_2) stretching vibration appeared at 1218 cm^{-1}, while for the GDP, the groups of bands in the 1750-1500 cm^{-1} region were assigned to the C=O and the C-C skeletal stretching[40,41]. The absorption peaks in the FTIR spectra of the chitosan sponges exhibited the presence of these characteristic bands of both ADP and GDP, confirming the incorporation of the purines within the chitosan structure (**Error! Reference source not found.**C).

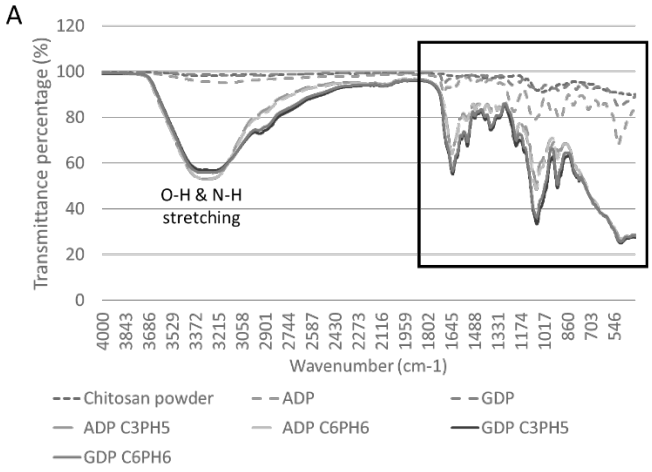

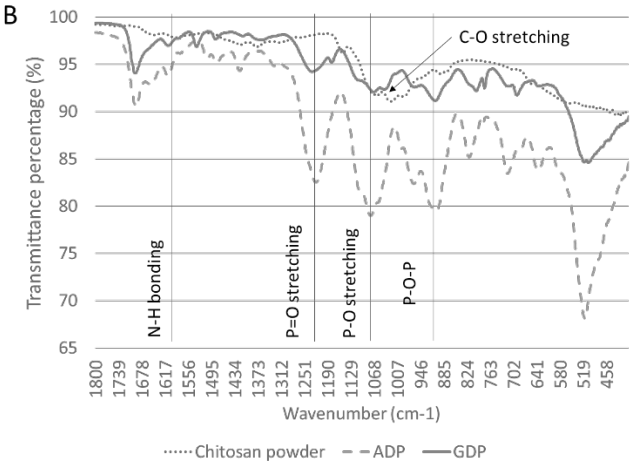

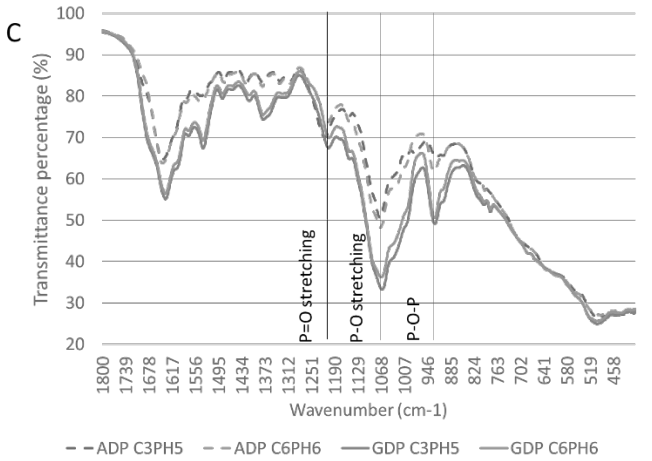

D

%	Raw powders	C3PH5	C6PH6
ADP	1.07	6.27	29.28
GDP	9.43	18.58	21.87
Chitosan	12.81		

Figure 2. FTIR Spectra, transmittance percentage (%) of all raw powders and sponges (A) with a zoom on wavenumbers below 1800 cm-1 for chitosan, ADP and GDP raw powders (B) and for the chitosan sponges with different compositions (C). Degree of crystallinity (%) obtained with XRD analysis (D).

First, the peaks corresponding to the P=O group became weaker (shifted from 1222 cm^{-1} to 1218 cm^{-1} and 1205 cm^{-1}, respectively) in ADP and GDP sponges as a result of cross-linking of the amine groups of chitosan with the phosphate groups of GDP and ADP. Secondly, the C3PH5 and C6PH6 formulations produced a similar spectrum with no detectable

changes in the peak intensities of the participating groups, suggesting that the pH and the concentration of chitosan did not play a major role in the sponge formation as long as the cross-linking process could occur. Indeed, at pH below its pKa (pH ≤ 6), the chitosan becomes a cationic polyelectrolyte due to the protonation of the free amino groups[42]. The sponges are then formed by ionic cross-linking between the positively charged amine groups of chitosan molecules and negatively charged phosphates groups of both the nucleotides ADP and GDP.

The solid-state ^{13}C-NMR analyses of different sponges (Figure 3) indicated very similar spectral behaviours between C3PH5 and C6PH6 (Figure 3A).

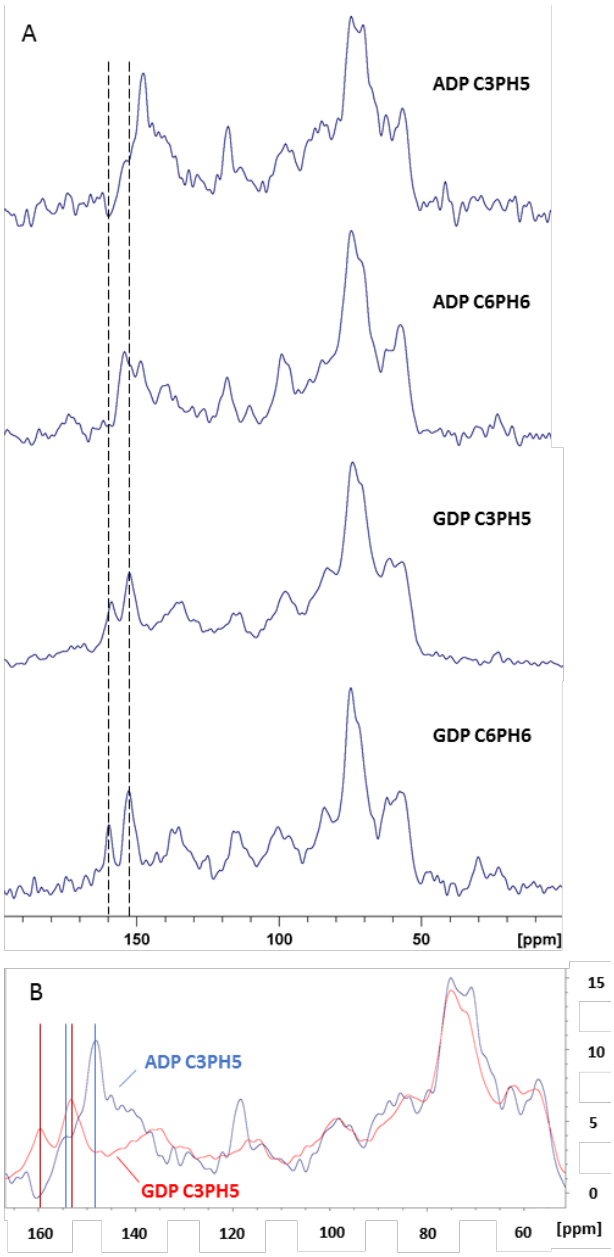

Figure 3. ^{13}C-NMR spectra of the chitosan sponges. A: All samples. B: Comparison between ADP- and GDP-C3PH5.

Further comparison between ADP and GDP for a single composition (Figure 3B) highlighted, on the one hand, a strong correlation for the peaks in the 50-100 ppm region (associated with carbon atoms from the chitosan chains[43,44]), and on the other hand, differences in peak locations between ADP and GDP for the 150 ppm region (associated with aromatic groups of the purines[45]). Such changes could be explained by different structural configurations between ADP and GDP after cross-linking. The cross-linked structure expected for the ADP-based sponge is shown on Figure 4A. Indeed, the predicted spectrum for this polymerized chain obtained with the ^{13}C-NMR prediction tool of the Mnova software (MestReNova 11.0.4, Mestrelab Research) was very similar to our experimental data (Supplementary Information S1). In contrast, the predicted spectrum of chitosan cross-linked with GDP in the same configuration as Figure 4A, was not consistent with our ^{13}C-NMR experimental data and did not show the shifts around 150 ppm noticed on Figure 3B. This would confirm that another molecular structure could appear in the GDP-based sponges.

Our postulation is that there is a bridge bonding between the guanine molecules, a component of GDP, to form a G-tetrad-like structure through Hoogsteen hydrogen bonds[46] (Figure 4B). This structure could participate in the formation of a three-dimensional network of guanine, providing more phosphate groups to interact electrostatically with chitosan, thereby forming the chemical bonds that stabilize the structure. Conversely, the sponge structure could be influenced by other secondary interchain interactions involving NH_2 group (in C_6) of ADP. The latter can participate via its positive charge to increase the electrostatic repulsion between the protonated amines and consequently between chitosan and ADP molecules, thereby affecting the microstructure of the sponge. Indeed, the predicted C-NMR spectrum for the quadruplex structure showed shifts in peaks around 150 ppm, similar to our experimental data, related to the aromatic carbon atoms C1 and C2 highlighted in Figure 4B. The XRD analysis (Figure 2D) revealed different degrees of crystallinity for the commercial powders and the different sponge formulation (Supplementary Information S2). As a result of cross-linking, the crystallinity of the formed sponge was higher than the raw materials. Moreover, although the maximal value was obtained for ADP C6PH6, GDP samples showed overall higher degrees of crystallinity (from 3 to 8 times higher compared to C3PH5 ADP and raw ADP, respectively). As determined by ^{13}C-NMR, we believe that the more organized structure provided by Hoogsteen hydrogen bonds in chitosan cross-linked with GDP increased the degree of crystallinity for GDP based sponges.

Sponge microstructure is affected by the nature of the cross-linker

The differences in cross-linking mechanisms, as revealed by NMR, strongly affected the internal structure of the sponge. Macroscopically, the chitosan-based GDP sponges were spongier than those made with ADP, smaller in size and contracted for the same volume of reagents. The microstructure of chitosan sponges acquired by using µCT on randomly selected areas inside the scaffolds indicated different morphologies between GDP- and ADP-based

This journal is © The Royal Society of Chemistry 20xx

Please do not adjust margins

sponges (Figure 5A). Surface/volume ratio, pore connectivity and volume of closed pores also varied between the samples (Figure 5B).

This journal is © The Royal Society of Chemistry 20xx

Please do not adjust margins

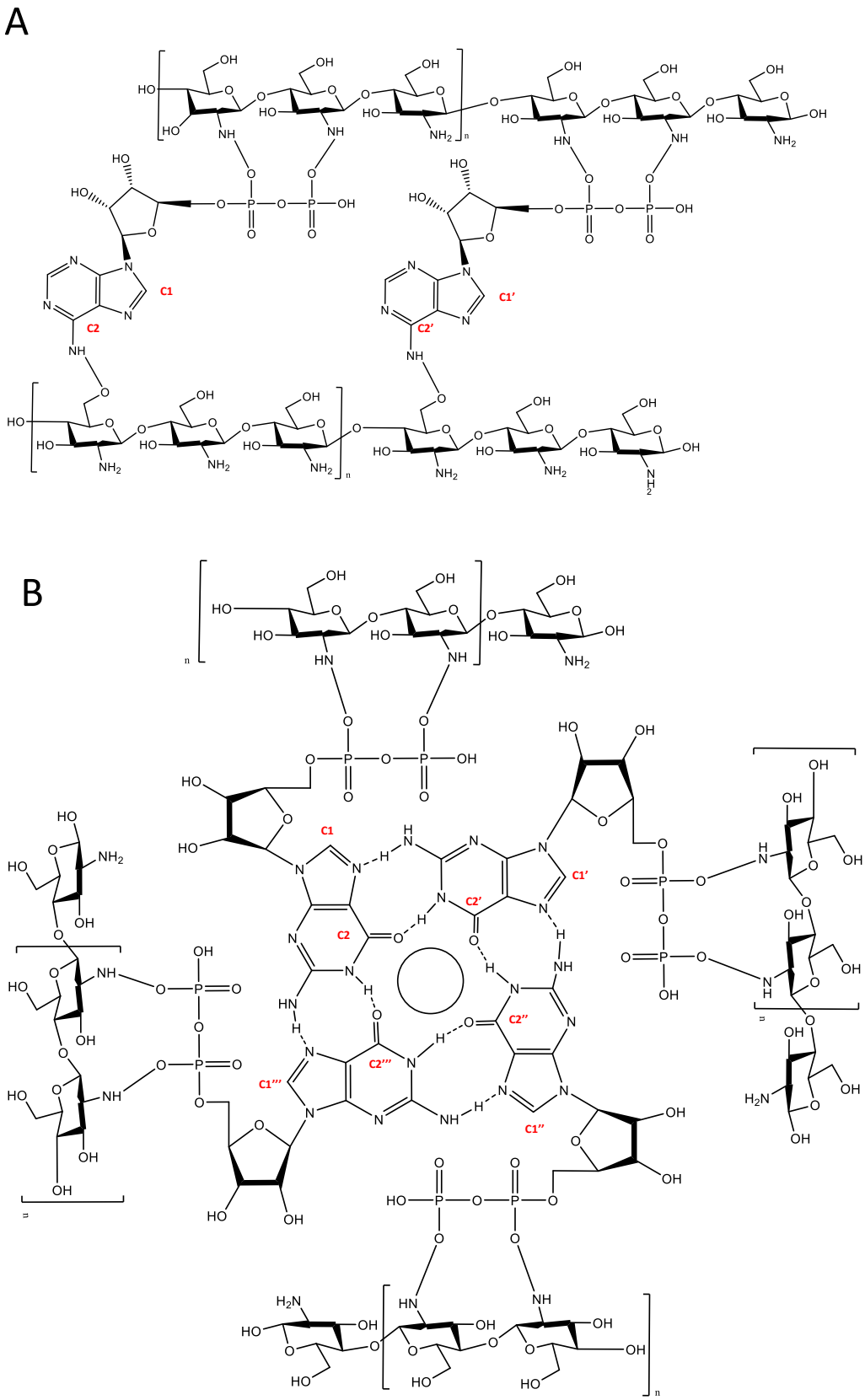

Figure 4. A: Structure of chitosan cross-linked with ADP. B: Structure of g-quadruplex created by the arrangement of four guanines through Hoogsteen hydrogen bonds in chitosan cross-linked with GDP.

This journal is © The Royal Society of Chemistry 20xx

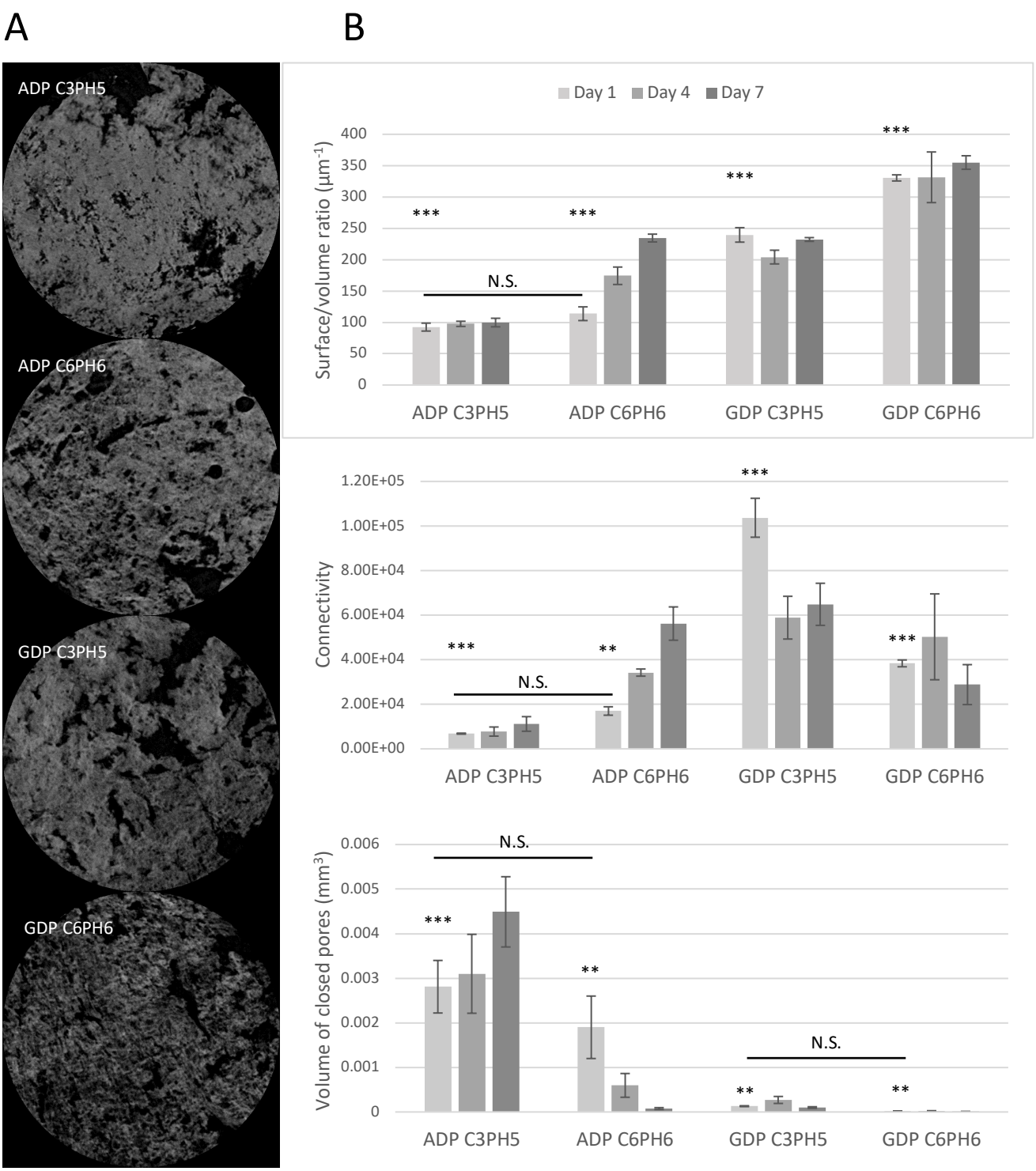

Figure 5. Results of the µCT measurements on sponges without encapsulated cells. A: Cross-sections of the internal structure of the sponges obtained after 3D reconstruction of the MicroCT acquisitions. Diameter 1.75mm. From top to bottom: ADP C3PH5 and C6PH6, GDP C3PH5 and C6PH6. B: Morphological properties. Significance was evaluated at day 1. N.S.: non-significant, **: p<0.01, ***: p<0.001.

An increase in pore connectivity over time could be noticed in some cases, possibly due to the progressive degradation of the scaffold. Indeed, the chitosan sponges are slowly degraded in water (few weeks to months) and small debris of chitosan gradually released from the outer layers result in increased pore connectivity. This is expected to connect the closed pores previously not connected, to the pore network and therefore to increase pore connectivity and to decrease

the volume of closed pores. The highest surface/volume ratio along with a small volume of closed pores ($1x10^{-5}$ mm^3) were found for GDP C6PH6 whereas the highest pore connectivity was observed for GDP C3PH5. These results strengthened our analysis of the cross-linking mechanisms, as the formation of quadruplex structure in the GDP-based sponges should lead to a more open structure and higher pore density, and therefore to a different overall porosity compared to ADP. The µCT measurements conducted on samples with encapsulated cells demonstrated a similar trend among the sponge formulations (Supplementary Information S3). Higher connectivity of GDP C3PH5 samples compared to GDP C6PH6 could be explained by sponges' bulk density, since the GDP C6PH6 sponges were prepared with twice more concentrated chitosan solution which resulted in denser scaffold with a volume comparable to GDP C3PH5 sponges. This lower density would also be consistent with the lower surface/volume ratio noticed for GDP C3PH5.

High surface/volume ratio and pore connectivity are crucial to ensure cell adhesion and infiltration, into or onto the scaffolds, and to facilitate the transport of nutrients and waste[47–51]. A small volume of closed pores is also needed to prevent the creation of population of cells not directly connected to the surrounding environment. Therefore, we expected that the more porous GDP-based sponges will offer an improved environment to ensure cell growth, development and viability after encapsulation. Moreover, the high degree of crystallinity of GDP C3PH5 compared to ADP C3PH5 (**Error! Reference source not found.**) was also expected to alter the cell behaviour. In a previous study by Freeman *et al*[52], the *in vivo* bone response to glass-ceramics implants showed a correlation with the crystallization. Effects on adhesion and proliferation of osteoblastic cells were also noticed *in vitro* and were explained by differences in integrin interactions with the surface as the surface roughness was affected by the degree of crystallinity[53–55]. For MC-3T3, in particular, orientation and patterning of the cells, and further their differentiation and functionality, could be linked to the scaffold crystallization[56]. Foster *et al*[57] also showed a correlation between increase in cell proliferation and increase in degree of crystallinity on chitosan samples (for non-bone cell population). We therefore analysed the biological response of encapsulated pre-osteoblasts MC-3T3 in our different scaffold formulations.

The nature of the cross-linker influences osteoblast MC-3T3 cells' viability and morphology

Figure 6 shows the metabolic activity of the encapsulated cells into ADP- or GDP-based chitosan sponges, as determined by the Alamar blue assay. Similar fluorescence intensities on days 1, 4, and 7 were obtained for C3PH5 and C6PH6 with the same cross-linker, indicating the negligible effect of chitosan concentration or pH on cell response. However, a significant increase in cell metabolic activity was measured at all time points with the GDP-based chitosan sponges compared to those made with ADP. As expected, following the study of the internal morphology and degree of crystallinity, cells in GDP C3PH5 showed a six- fold increase in comparison to ADP C3PH5 formulation activity ($p < 0.05$ to 0.001) at days 4 and 7. This difference in cell activity was more pronounced ($p < 0.01$ to 0.001) with the GDP C6PH6 formulation for all time points compared to the ADP C6PH6 formulation.

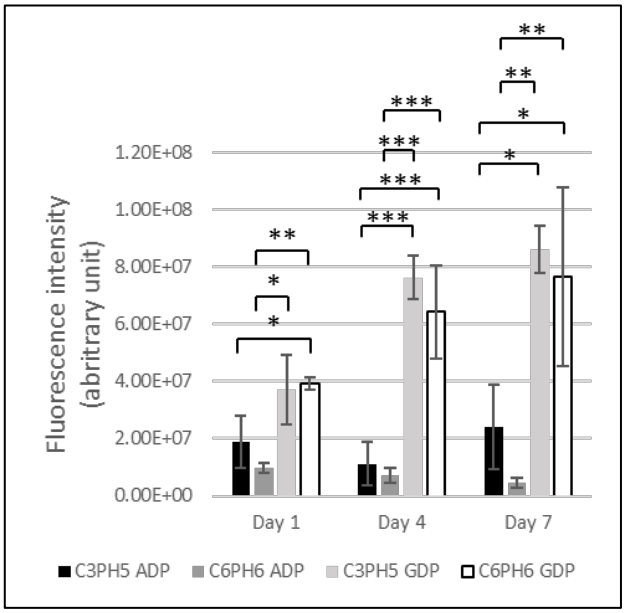

Figure 6. Metabolic activity by Alamar Blue assay of encapsulated pre-osteoblastic MC-3T3 cells in chitosan sponges at different time points (*: $p<0.05$, **: $p<0.01$, ***: $p<0.001$). Results were normalized by DNA content.

The SEM analyses confirmed the trend observed for the metabolic activity of MC-3T3 (Figure 7). The GDP-based chitosan scaffolds (both C3PH5 and C6PH6 formulations) clearly exhibited higher cell density and promoted more extra cellular matrix formation than ADP-based chitosan scaffolds.

The combination of the more suitable structural parameters, i.e., surface/volume ratio, pore connectivity and openness, as well as mechanical stability and surface roughness induced through a higher degree of crystallinity, created a more favourable environment and promoted MC-3T3 cell growth and attachment in GDP-based sponges compared to ADP samples. As a result, cells adopted an elongated fibroblast-like morphology that tended to create cellular layers on the porous structure of the sponge, whereas on the ADP formulations, the cells showed a spheroid-like structure highlighting a low attachment and less pronounced formation of cell tissue (Figure 7).

This journal is © The Royal Society of Chemistry 20xx

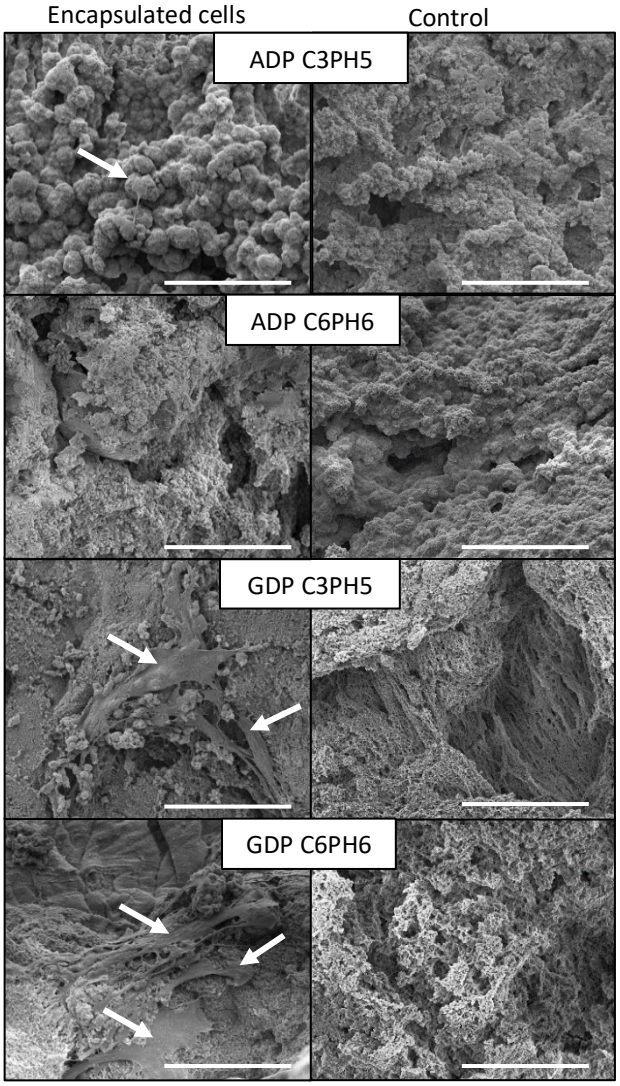

Figure 7. SEM micrographs of different chitosan sponges after 4 days with encapsulated pre-osteoblastic cells (left). Blank sponges without cells were used as control (right). Scale bar: 50 µm. Arrows: cell tissue.

Similar observations of cell morphology were noticed in confocal fluorescence images. In the GDP formulations, the spreading area of encapsulated MC-3T3 was distinctly larger than the ADP-containing sponges (Figure 8). At all time points, F-actin staining of cells by phalloidin displayed a connected network structure and a spreading cell behaviour on GDP formulations, although it was less pronounced after 7 days on the GDP C6PH6 sponge. In contrast, pre-osteoblastic cells encapsulated in the ADP sponges adopted a spherical morphology, which resulted in less intensity of the cytoskeleton staining.

In order to ensure that the differences in cell behaviour between ADP- and GDP-based sponges were not caused by a non-uniform distribution of the cells during the gelation process within the sponge, frozen slices of sponges were stained with DAPI directly on microscope slides and samples were observed by fluorescence microscopy (Supplementary Information S4).

CONCLUSION

In this work, we introduced ADP- and GDP-based chitosan sponges varying in chitosan concentration, pH and the type of cross-linker for cell encapsulation. Physicochemical analyses by FTIR and NMR and the study of cross-linking mechanisms allowed to conclude on the presence of Hoogsteen hydrogen bonds between the guanine molecules of GDP and the formation of quadruplex structure in chitosan cross-linked with GDP. The analysis of the bulk micro architecture with µCT confirmed this first finding, as the GDP-based sponges showed higher open porosity and pore connectivity than ADP-based scaffolds. The biological characterization of MC-3T3 cells encapsulated in these sponges validated the feasibility of the process and showed active, proliferative and homogeneously-distributed cells over time. As expected, the biological assessment of encapsulated cells tended to prove that the GDP-based chitosan sponges provided a superior environment for cell growth and viability as compared to ADP-based sponges. This favourable biological milieu for cell proliferation was a result of a more open 3-D microstructure provided by differences in cross-linking mechanism of GDP and ADP to chitosan, as revealed by ^{13}C-NMR. Knowing that the ADP or GDP signalling pathway of osteogenesis is different, their use as ionic cross-linker to construct injectable chitosan-based scaffold provides a very promising microenvironment by varying one parameter at a time to investigate the bone cell response to chitosan-based biomaterials for bone tissue engineering. The signalling pathways of these two cross-linkers once they are bond to chitosan backbone require however further investigation to determine how these pathways affect the encapsulated cells' functions and the biomineralization process for the use of these scaffolds for bone tissue engineering applications.

Acknowledgements

The authors acknowledge the financial support of CIHR through POP-phase 1, and CIHR and NSERC through CHRP grants. The authors thank MITACS and ALIGO Innovation for providing the scholarship to TB and LB, Robin Stein for her help on NMR analysis, Dr Martin Pellicelli for the µCT training.

Conflicts of interest

There are no conflicts to declare.

This journal is © The Royal Society of Chemistry 20xx

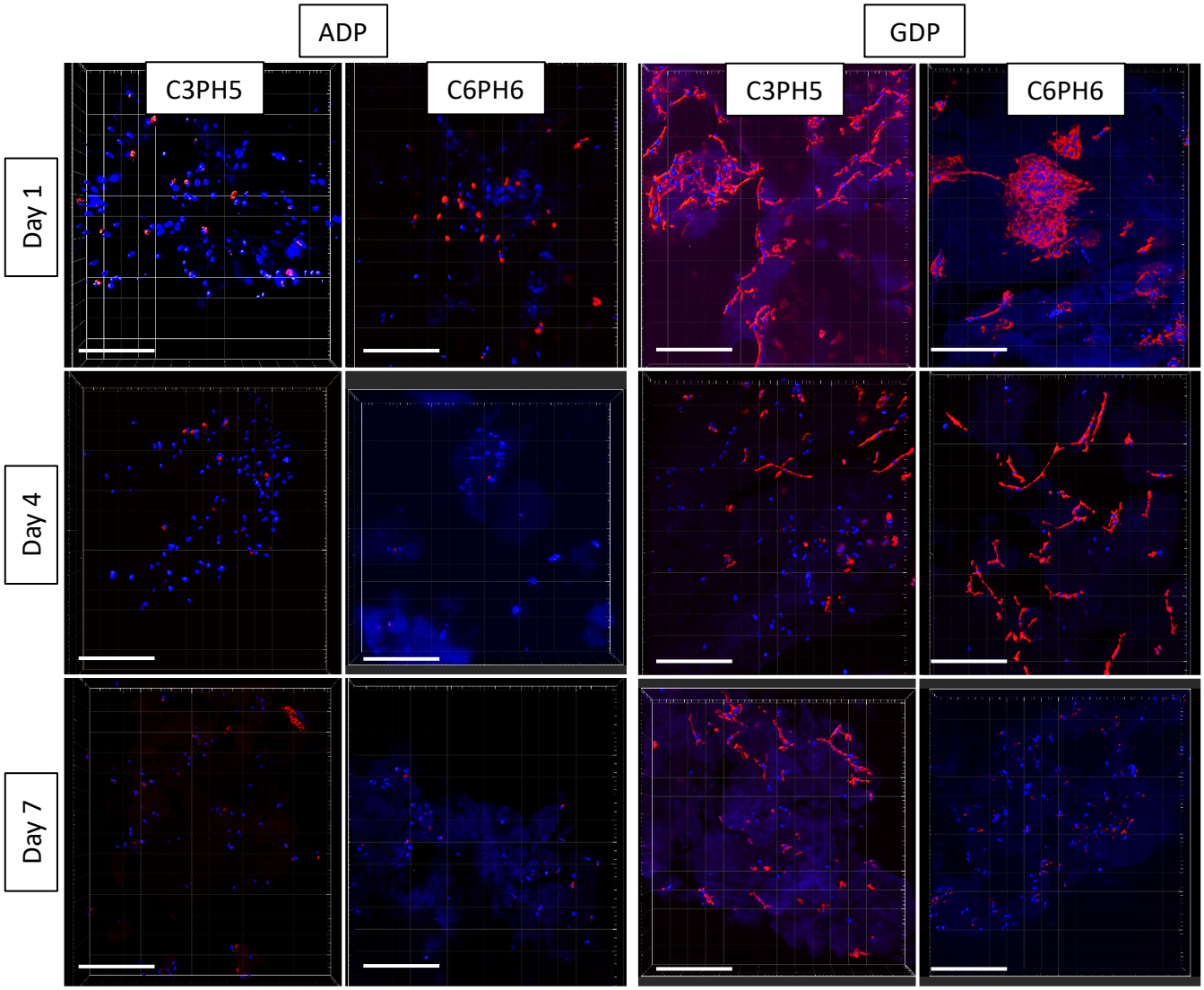

Figure 8. Confocal Microscopy pictures of the different chitosan sponges based on ADP (left) or on GDP (right) with encapsulated pre-osteoblastic cells after 1, 4 and 7 days. Scale bar: 200 µm.

This journal is © The Royal Society of Chemistry 20xx

Please do not adjust margins

References

1 A. Khademhosseini and R. Langer, *Nat. Protoc.*, 2016, **11**, 1775–1781.
2 X. Yin, B. E. Mead, H. Safaee, R. Langer, J. M. Karp and O. Levy, *Cell Stem Cell*, 2016, **18**, 25–38.
3 G. Orive, E. Santos, J. L. Pedraz and R. M. Hernández, *Adv. Drug Deliv. Rev.*, 2014, **67–68**, 3–14.
4 A. R. Amini, C. T. Laurencin and S. P. Nukavarapu, *Crit. Rev. Biomed. Eng.*, 2012, **40**, 363–408.
5 S. K. L. Levengood and M. Zhang, *J. Mater. Chem. B*, 2014, **2**, 3161.
6 D. Seliktar, *Science (80-.).*, 2012, **336**, 1124–1128.
7 K. Rezwan, Q. Z. Chen, J. J. Blaker and A. R. Boccaccini, *Biomaterials*, 2006, **27**, 3413–31.
8 J. Lee, M. J. Cuddihy and N. A. Kotov, *Tissue Eng. Part B Rev.*, 2008, **14**, 61–86.
9 N. Bhattarai, J. Gunn and M. Zhang, *Adv. Drug Deliv. Rev.*, 2010, **62**, 83–99.
10 M. Mekhail and M. Tabrizian, *Adv. Healthc. Mater.*, , DOI:10.1002/adma.
11 M. Rodríguez-Vázquez, B. Vega-Ruiz, R. Ramos-Zúñiga, D. A. Saldaña-Koppel and L. F. Quiñones-Olvera, *Biomed Res. Int.*, 2015, **2015**, 1–15.
12 C. Xu, X. Han, Y. Jiang, S. Yuan, Z. Wu, Z. Wu and X. Qi, *Bioconjug. Chem.*, 2017, acs.bioconjchem.7b00324.
13 G. Berth, H. Dautzenberg and M. G. Peter, *Carbohydr. Polym.*, 1998, **36**, 205–216.
14 M. N. V. R. Kumar, R. A. A. Muzzarelli, C. Muzzarelli, H. Sashiwa and A. J. Domb, *Chem. Rev.*, 2004, **104**, 6017–6084.
15 B. K. Singh, R. Sirohi, D. Archana, A. Jain and P. K. Dutta, *Int. J. Polym. Mater. Polym. Biomater.*, 2015, **64**, 242–252.
16 R. Kumari and P. K. Dutta, *Int. J. Biol. Macromol.*, 2010, **46**, 261–266.
17 M. Mekhail, K. Jahan and M. Tabrizian, *Carbohydr. Polym.*, 2014, **108**, 91–98.
18 M. Mekhail, J. Daoud, G. Almazan and M. Tabrizian, *Adv Heal. Mater*, 2013, **2**, 1126–1130.
19 L. Nayef, M. Mekhail, L. Benameur, J. S. Rendon, R. Hamdy and M. Tabrizian, *Acta Biomater.*, 2015, 1–9.
20 E. Ruel-Gariépy and J.-C. Leroux, *Eur. J. Pharm. Biopharm.*, 2004, **58**, 409–426.
21 A. Chenite, C. Chaput, D. Wang, C. Combes, M. . Buschmann, C. . Hoemann, J. . Leroux, B. . Atkinson, F. Binette and A. Selmani, *Biomaterials*, 2000, **21**, 2155–2161.
22 C. R. Nuttelman, S. M. Henry and K. S. Anseth, *Biomaterials*, 2002, **23**, 3617–26.
23 L. Wang and J. P. Stegemann, *Biomaterials*, 2010, **31**, 3976–3985.
24 P. Mukhopadhyay, K. Sarkar, S. Bhattacharya, A. Bhattacharyya, R. Mishra and P. P. Kundu, *Carbohydr. Polym.*, 2014, **112**, 627–637.
25 J. Berger, M. Reist, J. M. Mayer, O. Felt, N. A. Peppas and R. Gurny, *Eur. J. Pharm. Biopharm.*, 2004, **57**, 19–34.
26 M. Mekhail, G. Almazan and M. Tabrizian, *Biomater. Sci.*, 2015, **3**, 279–287.
27 G. Orive, R. M. Hernández, A. R. Gascón, R. Calafiore, T. M. S. Chang, P. De Vos, G. Hortelano, D. Hunkeler, I. Lacík, A. M. J. Shapiro and J. L. Pedraz, *Nat. Med.*, 2003, **9**, 104–107.
28 G. Orive, E. Santos, D. Poncelet, R. M. Hernández, J. L. Pedraz, L. U. Wahlberg, P. De Vos and D. Emerich, *Trends Pharmacol. Sci.*, 2015, **36**, 537–546.
29 L. C. Strazzulla and B. N. Cronstein, *Purinergic Signal.*, 2016, **12**, 583–593.
30 J. Linden, *Mol. Pharmacol.*, 2005, **67**, 1385–1387.
31 K. M. Pettifer, S. Kleywegt, C. J. Bau, J. D. Ramsbottom, E. Vertes, R. Ciccarelli, F. Caciagli, E. S. Werstiuk and M. P. Rathbone, *Neuroreport*, 2004, **15**, 833–836.
32 G. Burnstock, T. R. Arnett and I. R. Orriss, *Purinergic Signal.*, 2013, **9**, 541–572.
33 H. Lv, T. Che, X. Tang, L. Liu and J. Cheng, *Mol. Med. Rep.*, 2015, **12**, 2283–2290.
34 R. L. Johnson and K. Schmidt-Rohr, *J. Magn. Reson.*, 2014, **239**, 44–49.
35 A. Sionkowska, M. Wisniewski, J. Skopinska, C. J. Kennedy and T. J. Wess, *Biomaterials*, 2004, **25**, 795–801.
36 W. W. Thein-Han and R. D. K. Misra, *Acta Biomater.*, 2009, **5**, 1182–97.
37 A. Epp, T. Ramasarma and L. R. Wetter, *J. Am. Chem. Soc.*, 1958, **80**, 724–727.
38 J. H. Wang, D. G. Xiao, H. Deng, R. Callender and M. R. Webb, *Biospectroscopy*, 1998, **4**, 219–227.
39 A. Barth and W. Mäntele, *Biophys. J.*, 1998, **75**, 538–44.
40 T. Shimanouchi, M. Tsuboi and Y. Kyogoku, in *Advances in Chemical Physics: Structure & Properties of Biomolecules Vol. 7*, ed. J. Duchesne, John Wiley & Sons, Inc., Hoboken, NJ, USA, 1964, pp. 435–498.
41 R. P. Lopes, M. P. M. Marques, R. Valero, J. Tomkinson and L. A. E. B. de Carvalho, *Spectrosc. An Int. J.*, 2012, **27**, 273–292.
42 L. Vachoud, N. Zydowicz and A. Domard, *Carbohydr. Res.*, 1997, **302**, 169–177.
43 A. Domján, J. Bajdik and K. Pintye-Hódi, *Macromolecules*, 2009, **42**, 4667–4673.
44 H. Kono and T. Teshirogi, *Int. J. Biol. Macromol.*, 2015, **72**, 299–308.
45 F. Wang, R. Zhang, Q. Wu, T. Chen, P. Sun and A.-C. Shi, *ACS Appl. Mater. Interfaces*, 2014, **6**, 21397–21407.
46 P. Murat and S. Balasubramanian, *Curr. Opin. Genet. Dev.*, 2014, **25**, 22–29.
47 M. Mastrogiacomo, S. Scaglione, R. Martinetti, L. Dolcini, F. Beltrame, R. Cancedda and R. Quarto, *Biomaterials*, 2006, **27**, 3230–7.
48 D. F. Williams, *Biomaterials*, 2008, **29**, 2941–2953.
49 H. Petite, V. Viateau, W. Bensaïd, A. Meunier, C. de Pollak, M. Bourguignon, K. Oudina, L. Sedel and G. Guillemin, *Nat.*

Please do not adjust margins

Please do not adjust margins

Am., 2000, 959–963.
50 S. Lü, C. Gao, X. Xu, X. Bai, H. Duan, N. Gao, C. Feng, Y. Xiong and M. Liu, *ACS Appl. Mater. Interfaces*, 2015, **7**, 13029–13037.
51 W. Chen, S. Chen, Y. Morsi, H. El-Hamshary, M. El-Newhy, C. Fan and X. Mo, *ACS Appl. Mater. Interfaces*, 2016, **8**, 24415–24425.
52 C. O. Freeman, I. M. Brook, A. Johnson, P. V Hatton, R. G. Hill and K. T. Stanton, *J. Mater. Sci. Mater. Med.*, 2003, **14**, 985–90.
53 I. Bayer, *Materials (Basel).*, 2017, **10**, 748.
54 H. Yuan, Y. Zhou, M.-S. Lee, Y. Zhang and W.-J. Li, *Acta Biomater.*, 2016, **42**, 247–257.
55 N. Yui, K. Sanui, N. Ogata, K. Kataoka, T. Okano and Y. Sakurai, *J. Biomed. Mater. Res.*, 1983, **17**, 383–388.
56 W. Li, L. Lu, Y. Jiao, C. Zhang and C. Zhou, *J. Biomater. Sci. Polym. Ed.*, 2016, **27**, 1317–1330.
57 L. J. R. Foster, S. Ho, J. Hook, M. Basuki and H. Marçal, *PLoS One*, 2015, **10**, e0135153.
58 T. Albrektsson and C. Johansson, *Eur Spine J*, 2001, 96–101.

 This journal is © The Royal Society of Chemistry 20xx

Please do not adjust margins